# 

Cite as: Appl. Phys. Lett. **116**, 012404 (2020); https://doi.org/10.1063/1.5129548 Submitted: 30 September 2019 . Accepted: 16 December 2019 . Published Online: 06 January 2020

Tao Wang (10), Sergi Lendinez (10), M. Benjamin Jungfleisch (10), James Kolodzey (10), John Q. Xiao, and Xin Fan (10)

## COLLECTIONS



This paper was selected as an Editor's Pick







## ARTICLES YOU MAY BE INTERESTED IN

Non-magnetic origin of spin Hall magnetoresistance-like signals in Pt films and epitaxial NiO/Pt bilayers

Applied Physics Letters 116, 022410 (2020); https://doi.org/10.1063/1.5134814

Sensing anisotropic stresses with ferromagnetic nanowires
Applied Physics Letters 116, 013104 (2020); https://doi.org/10.1063/1.5132539

Large anomalous Hall effect in L1<sub>2</sub>-ordered antiferromagnetic Mn<sub>3</sub>Ir thin films Applied Physics Letters 116, 022408 (2020); https://doi.org/10.1063/1.5128241









# 

Cite as: Appl. Phys. Lett. **116**, 012404 (2020); doi: 10.1063/1.5129548 Submitted: 30 September 2019 · Accepted: 16 December 2019 · Published Online: 6 January 2020







Tao Wang,<sup>1</sup> no Sergi Lendinez,<sup>2</sup> no M. Benjamin Jungfleisch,<sup>2</sup> no James Kolodzey,<sup>1</sup> no John Q. Xiao,<sup>2,a)</sup> and Xin Fan<sup>3,a)</sup> no

### **AFFILIATIONS**

- <sup>1</sup>Department of Electrical and Computer Engineering, University of Delaware, Newark, Delaware 19716, USA
- <sup>2</sup>Department of Physics and Astronomy, University of Delaware, Newark, Delaware 19716, USA
- <sup>3</sup>Department of Physics and Astronomy, University of Denver, Denver, Colorado 80210, USA

### **ABSTRACT**

It has been recently demonstrated that spin-orbit coupling in ferromagnetic metals can generate spin current with symmetries different from the conventional spin Hall effect in nonmagnetic metals. The generated spin current can induce a spin-orbit torque on a neighboring magnetic layer with spin rotation symmetry. In this paper, we introduce a set of tools to measure this effect in a perpendicularly magnetized film, by using the second-order planar Hall effect method and spin-torque ferromagnetic resonance spectroscopy. These results are comparable to those detected by the polar magneto-optic Kerr effect technique.

Published by AIP Publishing. https://doi.org/10.1063/1.5129548

The spin Hall effect (SHE)<sup>1-3</sup> enables conversion from an electric current into a spin current within a nonmagnet (NM). It exerts a spin–orbit torque (SOT)<sup>4,5</sup> on a neighboring ferromagnet (FM), which can be used to switch magnetization,<sup>6,7</sup> and drive motion of magnetic domain walls<sup>8,9</sup> and skyrmions<sup>10,11</sup> in applications of magnetic memories. The SHE has a symmetry such that the electric current, spin current, and spin direction are all orthogonal to each other. Limited by this symmetry, an in-plane electric current can only generate an out-of-plane spin current when the spin direction is within the film plane, which sets a constraint on practical applications. For example, to deterministically switch a perpendicularly magnetized film using an in-plane polarized spin current, an external magnetic field or equivalent field is often required.<sup>12–15</sup> Thus, it is desirable to exploit unconventional spin–orbit coupling mechanisms that allow the manipulation of the spin direction.

Recent work has shown that the limitation of the conventional spin Hall symmetry can be lifted by breaking additional symmetry of spin current generators. MacNeil and Stiehl *et al.* have demonstrated that crystal symmetry can be used to control SOT directions in WTe<sub>2</sub>/FM bilayers. Taniguchi *et al.* have proposed to use a magnetic film with magnetization partially tilted out-of-plane. Due to the spin filtering effect, it is expected that the SHE from the magnetic film will generate a spin current with spin direction parallel to the magnetization. Humphries and Wang *et al.* have observed a spin-charge

conversion with spin rotation symmetry in a magnetic film, <sup>18</sup> in which an unconventional spin current is generated with spin direction perpendicular to both the magnetization and the spin direction due to the conventional SHE. Hereafter, we refer to the generation of spin current with spin rotation symmetry from a magnetic film as the spin rotation effect. It can be used to generate an out-of-plane polarized spin current, <sup>19</sup> by using an in-plane magnetized film. Due to the simple device architecture and magnetization-dependent spin current generation, the spin rotation effect becomes a promising candidate for generating spin current with arbitrary spin direction.

While the spin rotation effect has been demonstrated by both experiments <sup>18,19</sup> and first principles calculations, <sup>20</sup> the underlying mechanisms for the spin rotation effect are still unsettled. Two different theories have been postulated that lead to the spin rotation effect, including the spin–orbit precession <sup>19,21</sup> at the interface between the ferromagnetic and the neighboring nonmagnetic layer, and the spin swapping effect due to the extrinsic spin–orbit scattering in the bulk ferromagnet. <sup>22,23</sup> In order to investigate different microscopic mechanisms and to search for magnetic material systems that exhibit efficient spin rotation effect, it is important to develop sensitive and convenient tools to quantify this effect.

A general device for studying the spin rotation effect is a FM1/NM/FM2 spin valve structure, where the FM1 layer is the ferromagnetic spin current generator. The spin current diffuses through the

<sup>&</sup>lt;sup>a)</sup>Authors to whom correspondence should be addressed: xin.fan@du.edu and jqx@udel.edu

NM spacer layer and exerts a SOT on the FM2 layer, which serves as a spin detector of the spin current generated by the FM1 via the spin rotation effect.

In this paper, we develop and compare a series of experimental procedures to measure SOTs generated by the spin rotation effect in a perpendicularly magnetized film. We show that the second-order planar Hall effect (PHE), <sup>24,25</sup> spin-torque ferromagnetic resonance (ST-FMR), <sup>26</sup> and magneto-optic Kerr effect (MOKE), <sup>27,28</sup> which were developed for studying regular SOTs with spin Hall symmetry in NM/FM bilayers, can be applied to study the SOTs with spin rotation symmetry.

Generally, the spin current is a tensor with two spatial indices,  $Q_{\alpha\beta} \propto v_{\alpha} \otimes S_{\beta}$ : subscript  $\alpha$  specifies the spin current flow direction and superscript  $\beta$  specifies the spin direction, where  $v_{\alpha}$  is the spin velocity operator,  $S_{\beta}$  is the Pauli spin matrix, and  $\alpha$ ,  $\beta \in [x, y, z]$ . In this paper, it is only the spin current flowing in the z-direction that is of interest, we can reduce the spin current tensor to a vector,  $\mathbf{Q}_{z}$ , in the notation of which the magnitude of the vector represents the magnitude of the spin current, and the direction represents the spin polarization orientation. As shown in Fig. 1(a), when applying an in-plane electric field  $\mathbf{E}$  to a FM layer with perpendicular magnetization  $\mathbf{m}$ , a spin current can be generated via spin–orbit coupling that flows out of plane which can be described as  $^{29}$ 

$$\mathbf{Q}_{z} = \mathbf{Q}_{SH} + \mathbf{Q}_{SR} = \sigma_{SH}(\hat{\mathbf{z}} \times \mathbf{E}) + \sigma_{SR}\mathbf{m} \times (\hat{\mathbf{z}} \times \mathbf{E}), \quad (1)$$

where  $\mathbf{m}$  is the unit magnetization vector. In the rest of the paper, we refer to the first term on the right as the spin-Hall-spin current  $\mathbf{Q}_{\text{SH}}$ , and the second term as the spin-rotation-spin current  $\mathbf{Q}_{\text{SR}}$ , with  $\sigma_{\text{SH}}$  and  $\sigma_{\text{SR}}$  being the corresponding spin Hall conductivities. According to Eq. (1), the spin direction of  $\mathbf{Q}_{\text{SH}}$  remains the same when the magnetization switches, while that of  $\mathbf{Q}_{\text{SR}}$  reverses as  $\mathbf{m}$  switches, as illustrated in Fig. 1(a). The different directions and dependences on the magnetization can be used to distinguish the spin Hall and spin rotation spin current components.

Figure 1(b) shows a schematic of the sample used for this study. The complete layer stack is GaAs/Ta (4.0)/Pt (3.0)/Co (0.7)/Cu (3.0)/Py (3.0)/Pt (3.0) (unit in parentheses: nm,  $Py = Ni_{80}Fe_{20}$ ). All layers were fabricated by magnetron sputtering in a 3.0 mTorr Ar environment.

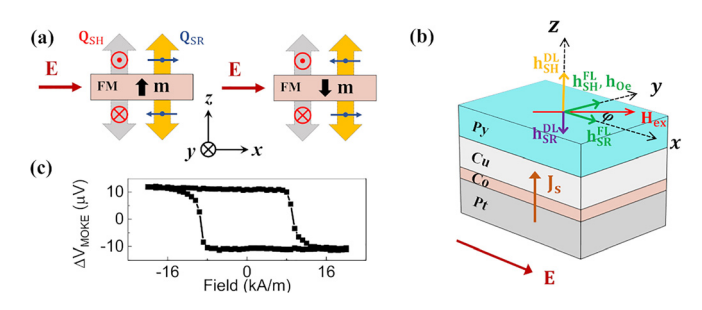


**FIG. 1.** Spin-orbit effects with spin Hall and spin rotation symmetries. (a) Spin currents generated from a FM layer by an in-plane electrical field  ${\bf E}$ . The gray arrows represent the conventional spin-Hall-spin current  ${\bf Q}_{SH}$ , and the orange arrows denote the spin-rotation-spin current  ${\bf Q}_{SR}$ , with their corresponding spin directions marked by red and blue colors, respectively.  ${\bf Q}_{SR}$  depends on the orientation of the FM magnetization  ${\bf m}$ , which is indicated by a black arrow. (b) The film stack of the Pt/Co/Cu/Py spin valve sample (Pt capping layer is not shown). (c) Out-of-plane hysteresis loop of the sample measured by the polar MOKE.

The base pressure was lower than  $2 \times 10^{-7}$  Torr before sputtering. Here, Py has an easy axis in-plane, and Co is a perpendicularly magnetized layer (PML). As shown in Fig. 1(c), out-of-plane magnetization hysteresis was characterized by polar-MOKE magnetometry, indicating nearly 100% remanence of the PML.

We expect the spin current  $\mathbf{Q}_z$  generated from the Co layer to have a  $\mathbf{Q}_{SH}$  component with spin in the *y*-direction and a  $\mathbf{Q}_{SR}$  component with spin in the *x*-direction. Both  $\mathbf{Q}_{SH}$  and  $\mathbf{Q}_{SR}$  can generate dampinglike (DL-) and fieldlike (FL-) SOTs on Py magnetization. Their corresponding effective fields are: (1)  $\mathbf{h}_{SH}^{DL} = \xi_{SH}^{DL} \frac{\hbar}{2e\mu_0 M_{Py} d_{Py}} (\mathbf{m}_{Py} \times \mathbf{Q}_{SH})$ ; (2)  $\mathbf{h}_{SH}^{FL} = \xi_{SH}^{FL} \frac{\hbar}{2e\mu_0 M_{Py} d_{Py}} \mathbf{Q}_{SH}$ ; (3)  $\mathbf{h}_{SR}^{DL} = \xi_{SR}^{DL} \frac{\hbar}{2e\mu_0 M_{Py} d_{Py}} (\mathbf{m}_{Py} \times \mathbf{Q}_{SR})$ ; and (4)  $\mathbf{h}_{SR}^{FL} = \xi_{SR}^{FL} \frac{\hbar}{2e\mu_0 M_{Py} d_{Py}} \mathbf{Q}_{SR}$ . Here,  $\hbar$  is the reduced Planck constant, e is the electron charge,  $\mathbf{m}_{Py}$ ,  $\mu_0 M_{Py}$ , and  $d_{Py}$  are the unit magnetization vector, saturation magnetization, and thickness of the Py layer, respectively, and  $\xi_{SH}^{FL}$  ( $\xi_{SH}^{FL}$ ), and  $\xi_{SR}^{FL}$  ( $\xi_{SR}^{FL}$ ) are unitless charge to spin efficiencies of the spin Hall effect and spin rotation effect, respectively, which are sometimes referred to as effective spin Hall angles.  $^{7,30,31}$  It should be pointed out that an in-plane Oersted field ( $\mathbf{h}_{Oe}$ ) is also generated, which is collinear with  $\mathbf{h}_{SH}^{FL}$ .

We first measure the spin current induced FL-SOTs on the Py magnetization  $m_{\rm Py}$  with the second-order PHE technique, which is more sensitive to in-plane effective fields than out-of-plane ones due to the negligible anomalous Hall effect voltage applied on Py.<sup>24,25</sup> By applying an AC of 20 mA in a 50  $\mu$ m  $\times$  250  $\mu$ m Hall bar device at a frequency of 346 Hz, we detect the PHE voltage  $\Delta V_{\rm PHE}$  at twice the frequency:

$$\Delta V_{PHE} = I^2 \cdot \Delta R \cdot \chi_{\parallel} [H_{ex}] \cdot \frac{\partial h_{\parallel}}{\partial I}, \tag{2} \label{eq:delta-VPHE}$$

where  $\Delta R$  is due to the total anisotropic magnetoresistance (AMR),  $\chi_{\parallel}[H_{ex}] = \frac{1}{H_{ex}+H_{ani}}$  is an external field dependent susceptibility, where  $H_{ani}$  is the in-plane magnetic anisotropy field,  $^{25}$  and  $h_{\parallel}$  is the current-induced in-plane effective field including  $\mathbf{h}_{SH}^{FL}$ ,  $\mathbf{h}_{SR}^{FL}$ , and  $\mathbf{h}_{Oe}$ .

The FL-SOT due to  $\mathbf{Q}_{SH}$  is measured using the configuration shown in the inset of Fig. 2(a), where the external magnetic field  $\mathbf{H}_{ex}$  is applied parallel to the electric current I ( $\phi=0^{\circ},\phi$  is the angle between I and  $\mathbf{H}_{ex}$ ). In this case,  $\mathbf{h}_{SR}^{FL}=0$ , and  $\mathbf{h}_{\parallel}=\mathbf{h}_{SH}^{FL}+\mathbf{h}_{Oe}$ , both terms are independent of the Co layer ( $\mathbf{m}_{Co}$ ). Therefore, as shown in Fig. 2(a),  $\Delta V_{PHE}$  is the same when the Co layer is reversed from  $\mathbf{m}_{Co}=+\mathbf{z}$  to  $\mathbf{m}_{Co}=-\mathbf{z}$ . In the configuration  $\phi=90^{\circ}$ , shown in the inset of Fig. 2(b),  $\mathbf{Q}_{SH}$  has spin direction parallel with  $\mathbf{m}_{Py}$  at saturation; thus, both  $\mathbf{h}_{SH}^{FL}$  and  $\mathbf{h}_{Oe}$  do not contribute to magnetization reorientation.  $\mathbf{h}_{\parallel}$  can only arise from  $\mathbf{Q}_{SR}$  induced effective field  $\mathbf{h}_{SR}^{FL}$ . According to Eq. (1),  $\mathbf{h}_{SR}^{FL}$ , which arises from  $\mathbf{Q}_{SR}$ , should switch sign as  $\mathbf{m}_{Co}$  switches. This is confirmed by the measurement results shown in Fig. 2(b).

By calibrating the susceptibility  $\chi_{\parallel}[H_{ex}]$  with an external calibration field, we extrapolate  $h_{\parallel}(\phi=0^{\circ})=h_{SH}^{FL}+h_{Oe}=149\pm 8$  A/m in the spin-Hall-spin current configuration of Fig. 2(a) and  $h_{\parallel}(\phi=90^{\circ})=h_{SR}^{FL}=47\pm 7$  A/m in the spin-rotation-spin current configuration of Fig. 2(b). In this paper, we do not attempt to distinguish  $h_{SH}^{FL}$  from  $h_{Oe}$ , as they have the same symmetry and are always entangled in all detection techniques discussed in this paper.

The second-order PHE measurement is sensitive to FL-SOT, while the polar-MOKE is sensitive to DL-SOT. <sup>18,28</sup> An AC of 40 mA is applied through the MOKE sample ( $50 \mu m \times 50 \mu m$ ) at a frequency of

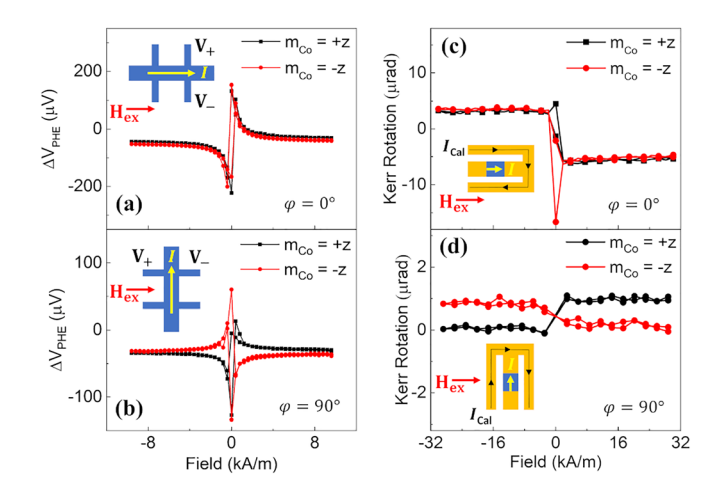


**FIG. 2.** Measurements of SOTs induced by spin-Hall-spin current and spin-rotation-spin current. The configurations of conventional spin Hall effect  $(\phi=0^\circ)$  and spin rotation effect  $(\phi=90^\circ)$  SOTs measurements, and their corresponding second-order PHE results (a) and (b) and polar-MOKE results (c) and (d), which indicate that the conventional spin-Hall spin current is independent of the orientation of PML magnetization  $\mathbf{m}_{\text{Co}}$ , but the spin-rotation spin current shows  $\mathbf{m}_{\text{Co}}$  dependency.

1777 Hz. The out-of-plane magnetization tilting, which is induced by AC generated DL-SOTs, modulates the light polarization as the light is reflected off the sample via the polar-MOKE, which is readout by a balanced detector locked into the AC frequency. Our previous work has demonstrated that the polar Kerr rotation  $\Delta\theta_k$  is a direct indication of the effective field from DL-SOT:  $^{28,33}$ 

$$\Delta\theta_k = \eta \cdot I \cdot \chi_{\perp}[H_{ex}] \cdot \frac{\partial h_{\perp}}{\partial I}, \qquad (3$$

where  $\eta$  is the polar-MOKE coefficient, the susceptibility  $\chi_{\perp}[H_{ex}]=1/(H_{ex}+M_{eff}).^{28,33}~M_{eff}=M_s-\frac{2K_{\perp}}{\mu_0 M_s}$  arises from the demagnetization effect, and  $h_{\perp}$  represents the current induced out-of-plane effective field.

The DL-SOT due to  $\mathbf{Q}_{SH}$  is measured by using the polar-MOKE, which is shown in Fig. 2(c) ( $\phi=0^{\circ}$ ). The polar Kerr rotation  $\Delta\theta_k$  resembles Py magnetization hysteresis, which is a typical signature of the MOKE-based DL-SOT measurement.  $\Delta\theta_k$  is proportional to the effective field  $\mathbf{h}_{SH}^{DL}$  that is independent of  $\mathbf{m}_{Co}$ . In the configuration  $\phi=90^{\circ}$ , shown in Fig. 2(d), the MOKE signal reverses as  $\mathbf{m}_{Co}$  switches, which is consistent with the effective field  $\mathbf{h}_{SR}^{DL}$  due to  $\mathbf{Q}_{SR}=\sigma_{SR}\mathbf{m}_{Co}\times(\hat{\mathbf{z}}\times\mathbf{E})$ , as described in Eq. (1).

To extrapolate the magnitudes of  $\mathbf{h}_{SH}^{DL}$  and  $\mathbf{h}_{SR}^{DL}$ , we calibrate the polar-MOKE coefficient by applying an out-of-plane Oersted field. The calibration field with a known value of  $h_{Cal} = 680$  A/m is generated by a calibration wire patterned around the sample with  $I_{cal} = 400$  mA current, as is shown in the inset of Figs. 2(c) and 2(d). We are able to extract the effective fields induced by DL-SOTs  $h_{\perp}(\phi=0^{\circ})=h_{SH}^{DL}=872\pm12$  A/m and  $h_{\perp}(\phi=90^{\circ})=h_{SR}^{DL}=50\pm4$  A/m, respectively.

Finally, we perform the ST-FMR measurement on this spin valve sample. As shown in Figs. 3(a) and 3(b). A radio frequency (RF) current  $I_{RF} = I_{RF0} \sin \omega t$  is applied across the sample strip (20  $\mu$ m  $\times$  50  $\mu$ m) along the x direction, with a nominal input power of 0 dBm. A lock-in amplifier and a bias tee are used to measure the rectified

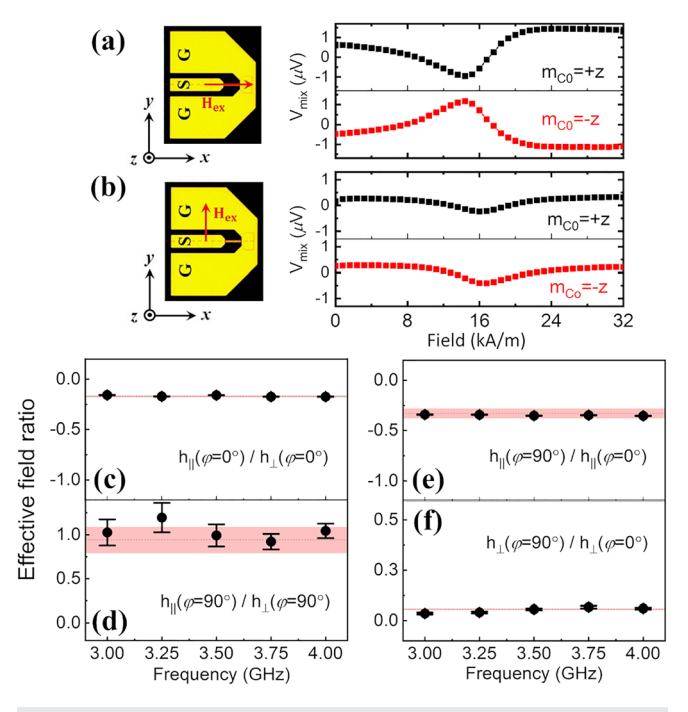


**FIG. 3.** ST-FMR measurement results. (a) The conventional spin-Hall as well as (b) the spin-rotation spin current induced rectified voltage when the PML magnetization  $\mathbf{m}_{\text{Co}}$  switches from +z to -z. (c)-(f) The effective field ratio comparison based on the second-order PHE, polar-MOKE, and ST-FMR results. The red shaded area is calculated with FL-SOT results from the second-order PHE measurement and DL-SOT results from the polar-MOKE measurement. The black data points indicate the ST-FMR results.

voltage. Sesides  $I_{RF}$  induced time-dependent change of AMR,  $\Delta R_{AMR}$ , there is also a contribution from giant magnetoresistance (GMR) oscillation,  $\Delta R_{GMR}$ , in this experiment. The rectified voltage contains symmetric and antisymmetric Lorentzian components, which are due to out-of-phase and in-phase RF magnetization, respectively. The in-plane effective fields  $\mathbf{h}_{||}$  on Py induce in-plane magnetization resonance  $\Delta m_{||}$ , which is in-phase with  $I_{RF}$  and contributes to the AMR change  $\Delta R_{AMR}$ .  $\mathbf{h}_{||}$  also induces out-of-plane magnetization oscillation  $\Delta m_{\perp}$ , which is out-of-phase with  $I_{RF}$  and contributes to the GMR oscillation  $\Delta R_{GMR}$ . Therefore,  $\mathbf{h}_{||}$  leads to an antisymmetric Lorentzian line shape in the AMR voltage  $V_{AMR}^{Asym}$ , but a symmetric Lorentzian GMR term  $V_{GMR}^{Sym}$ . In contrast, the out-of-plane effective field  $\mathbf{h}_{\perp}$  leads to a symmetric Lorentzian line shape in the AMR rectified voltage  $V_{AMR}^{Sym}$ , but an antisymmetric Lorentzian GMR term  $V_{GMR}^{Asym}$ . The voltage signals with different symmetries can be expressed as

$$V_{GMR}^{Asym}\!=\!\!\frac{1}{4}I_{RF}\Delta R_{GMR}\sqrt{\frac{1}{1\!+\!\left(H_{0}/H_{an\perp}\right)^{2}}\frac{\mu_{0}M_{Py}d_{Py}\sqrt{H_{0}/(H_{0}\!+\!M_{eff})}}{\alpha\gamma(2H_{0}\!+\!M_{eff})}}h_{\perp}, \label{eq:VGMR}$$

$$V_{GMR}^{Sym} = \frac{1}{4} I_{RF} \Delta R_{GMR} \sqrt{\frac{1}{1 + (H_0/H_{an\perp})^2}} \frac{\mu_0 M_{Py} d_{Py}}{\alpha \gamma (2H_0 + M_{eff})} h_{\parallel}, \quad (5)$$

$$V_{\rm AMR}^{\rm Asym} = \frac{1}{4} I_{\rm RF} \Delta R_{\rm AMR} \sin 2\phi \frac{\mu_0 M_{\rm Py} d_{\rm Py} \sqrt{1 + M_{\rm eff}/H_0}}{\alpha \gamma (2 H_0 + M_{\rm eff})} h_\parallel, \quad (6)$$

$$V_{AMR}^{Sym} = \frac{1}{4} I_{RF} \Delta R_{AMR} sin2 \varphi \frac{\mu_0 M_{Py} d_{Py}}{\alpha \gamma (2H_0 + M_{eff})} h_{\perp}, \tag{7}$$

where  $H_0$  is the ferromagnetic resonance (FMR) field.  $\alpha$  is the Gilbert damping coefficient and  $\gamma$  is the gyromagnetic ratio.  $H_{an\perp}=280\,k\text{A/m}$  is the effective perpendicular anisotropy field of the PML layer, which is determined by the vibrating sample magnetometer.  $\mu_0 M_{eff}=0.820\pm0.005\,$  T and  $\alpha=0.017\pm0.001\,$  are extracted from the additional FMR fitting procedure. According to Eq. (4)–(7), in configurations of both  $\phi=0^\circ$  and  $\phi=90^\circ$ , only the GMR components contribute to the rectified voltage  $V_{mix}$ , and the AMR induced rectified voltage is zero.

In configuration of  $\phi=0^\circ$ , the ratio of the in-plane and out-of-plane effective fields  $\frac{h_{\parallel}(\phi=0^\circ)}{h_{\perp}(\phi=0^\circ)}=\frac{h_{\rm SH}^{\rm H}+h_{\rm Oc}}{h_{\rm DH}^{\rm DL}}=\sqrt{H_0/(H_0+M_{\rm eff})}\frac{V_{\rm mix}^{\rm Sym}}{V_{\rm mix}^{\rm Asym}}$  at given frequency 3–4GHz, which is as shown in Fig. 3(c). For comparison, we calculate the same effective field ratio of  $\frac{h_{\parallel}(\phi=0^\circ)}{h_{\perp}(\phi=0^\circ)}=\frac{h_{\rm SH}^{\rm H}+h_{\rm Oc}}{h_{\rm BH}^{\rm DL}}=-0.17\pm0.01$  based on the second-order PHE and polar-MOKE measurements, which is marked with a red shadow area in Fig. 3(c). The good agreement indicates that these SOT measurement methods are consistent with each other.

In configuration of  $\phi=90^\circ$ , the ratio between in-plane and out-of-plane effective fields induced by the spin rotation symmetry  $\frac{h_{\parallel}(\phi=90^\circ)}{h_{\perp}(\phi=90^\circ)} = \frac{h_{SR}^{EL}}{h_{DR}^{EL}} = \sqrt{H_0/(H_0+M_{eff})} \frac{V_{mix}^{Nym}}{V_{mix}^{Nym}} \ \ \text{is shown in Fig. 3(d)}.$  Similarly,  $\frac{h_{\parallel}(\phi=90^\circ)}{h_{\perp}(\phi=90^\circ)} = 0.94 \pm 0.15 \ \ \text{is calculated based on previous}$  results at  $\phi=90^\circ$ . The other effective field ratios can also be extracted as  $\frac{h_{\parallel}(\phi=90^\circ)}{h_{\parallel}(\phi=0^\circ)} = \frac{h_{SH}^{EL}}{h_{SH}^{EL}+h_{Oc}} = -0.33 \pm 0.05 \ \ \text{and} \ \ \frac{h_{\perp}(\phi=90^\circ)}{h_{\perp}(\phi=0^\circ)} = \frac{h_{SH}^{DL}}{h_{SH}^{EL}} = -0.06 \pm 0.01.$  As shown in Figs. 3(e) and 3(f), the ST-FMR measurement result is highly consistent with that of the other SOTs measurements.

As mentioned previously, based on one parameter fitting to the resonance frequencies, the effective demagnetization field and the Gilbert damping show a good match with the magnetic properties of Py. In addition, the ultrathin Co layer on top of Pt tends to have much higher damping than Py.<sup>35</sup> The FMR response of Pt/Co under an inplane external field follows  $f = (\gamma/2\pi)[H_0(H_0 - M_{eff})]^{1/2}$ , which therefore indicates no Co resonance within the range of  $H_{ex} < 32\,\text{kA/m}$  in our experiment. Meanwhile, we estimate the RF current density is lower than  $1.0 \times 10^{10}~\text{A/m}^2$ . Thus, we expect that it can avoid the overheating issue in our ST-FMR study.

In summary, we demonstrate a series of experimental procedures, which can be used to quantitatively study the SOTs induced by spinrotation-spin current. We expect that these techniques will be useful
for understanding the spin rotation process as well as for developing
materials that exhibit a strong spin rotation effect for advanced spinorbitronics devices. In our experiment, the spin current generated by
the Pt/Co PML layer with spin Hall and spin rotation symmetries can
be detected and separated. The second-order PHE method is sensitive
to in-plane effective fields induced by FL-SOTs applied on FMs, especially the FMs that have larger PHE resistance than anomalous Hall
effect resistance. The polar-MOKE magnetometry directly probes the
out-of-plane magnetization component, which can simplify the SOT

extraction process without complications from PHE, AHE, and thermal effects. The ST-FMR based on AMR or even larger GMR could be a highly sensitive SOT detection technique, and more importantly, ST-FMR is a ferromagnetic resonance-based technique, which provides layer-resolved capability to separate contributions from different FM layers in FM1/NM/FM2 structures. However, in ST-FMR measurements, although the RF current calibration procedure has been demonstrated by different approaches, \$16,36,37\$ it is more challenging to determine the exact amount of RF current flowing through the sample than the AC currents in the second-order PHE and polar MOKE techniques, which are at much lower frequency. Moreover, the numerical fitting process in the ST-FMR method could potentially induce large error especially when the Lorentzian line shape contains a much stronger symmetric or antisymmetric component than its counterpart.

J.Q.X. acknowledges support from the NSF under Award No. DMR-1904076. M.B.J. acknowledges support from the NSF under Award No. 1833000.

### REFERENCES

<sup>1</sup>M. I. Dyakonov and V. I. Perel, Phys. Lett. A 35, 459 (1971).

<sup>2</sup>J. E. Hirsch, Phys. Rev. Lett. **83**, 1834 (1999).

<sup>3</sup>S. Zhang, Phys. Rev. Lett. **85**, 393 (2000).

<sup>4</sup>J. C. Slonczewski, J. Magn. Magn. Mater. **159**, L1 (1996).

<sup>5</sup>D. C. Ralph and M. D. Stiles, J. Magn. Magn. Mater. **320**, 1190 (2008).

<sup>6</sup>I. M. Miron, K. Garello, G. Gaudin, P.-J. Zermatten, M. V. Costache, S. Auffret, S. Bandiera, B. Rodmacq, A. Schuhl, and P. Gambardella, Nature 476, 189 (2011).

<sup>7</sup>L. Liu, C.-F. Pai, Y. Li, H. W. Tseng, D. C. Ralph, and R. A. Buhrman, Science 336, 555 (2012).

<sup>8</sup>I. M. Miron, T. Moore, H. Szambolics, L. D. Buda-Prejbeanu, S. Auffret, B. Rodmacq, S. Pizzini, J. Vogel, M. Bonfim, A. Schuhl, and G. Gaudin, Nat. Mater. 10, 419 (2011).

<sup>9</sup>S. Emori, U. Bauer, S.-M. Ahn, E. Martinez, and G. S. D. Beach, Nat. Mater. 12, 611 (2013).

<sup>10</sup>J. Sampaio, V. Cros, S. Rohart, A. Thiaville, and A. Fert, Nat. Nanotechnol. 8, 839 (2013).

<sup>11</sup>A. Fert, V. Cros, and J. Sampaio, Nat. Nanotechnol. **8**, 152 (2013).

<sup>12</sup>L. Liu, O. J. Lee, T. J. Gudmundsen, D. C. Ralph, and R. A. Buhrman, Phys. Rev. Lett. **109**, 096602 (2012).

<sup>13</sup>S. Fukami, C. Zhang, S. DuttaGupta, A. Kurenkov, and H. Ohno, Nat. Mater. 15, 535 (2016).

<sup>14</sup>Y.-C. Lau, D. Betto, K. Rode, J. M. D. Coey, and P. Stamenov, Nat. Nanotechnol. 11, 758 (2016).

<sup>15</sup>Y.-W. Oh, S.-H. Chris Baek, Y. M. Kim, H. Y. Lee, K.-D. Lee, C.-G. Yang, E.-S. Park, K.-S. Lee, K.-W. Kim, G. Go, J.-R. Jeong, B.-C. Min, H.-W. Lee, K.-J. Lee, and B.-G. Park, Nat. Nanotechnol. 11, 878 (2016).

<sup>16</sup>D. MacNeill, G. M. Stiehl, M. H. D. Guimaraes, R. A. Buhrman, J. Park, and D. C. Ralph, Nat. Phys. 13, 300 (2016).

<sup>17</sup>T. Taniguchi, J. Grollier, and M. D. Stiles, Phys. Rev. Appl. 3, 044001 (2015).

<sup>18</sup> A. M. Humphries, T. Wang, E. R. J. Edwards, S. R. Allen, J. M. Shaw, H. T. Nembach, J. Q. Xiao, T. J. Silva, and X. Fan, Nat. Commun. 8, 911 (2017).

<sup>19</sup>S. H. C. Baek, V. P. Amin, Y. W. Oh, G. Go, S. J. Lee, G. H. Lee, K. J. Kim, M. D. Stiles, B. G. Park, and K. J. Lee, Nat. Mater. 17, 509 (2018).

<sup>20</sup>F. Freimuth, S. Blügel, and Y. Mokrousov, *Phys. Rev. B* **98**, 024419 (2018).

<sup>21</sup>V. P. Amin, J. Zemen, and M. D. Stiles, Phys. Rev. Lett. **121**, 136805 (2018).

<sup>22</sup>M. B. Lifshits and M. I. Dyakonov, Phys. Rev. Lett. **103**, 186601 (2009).

<sup>23</sup>C. O. Pauyac, M. Chshiev, A. Manchon, and S. A. Nikolaev, Phys. Rev. Lett. 120, 176802 (2018).

<sup>24</sup>M. Hayashi, J. Kim, M. Yamanouchi, and H. Ohno, Phys. Rev. B 89, 144425 (2014).

25 X. Fan, J. Wu, Y. Chen, M. J. Jerry, H. Zhang, and J. Q. Xiao, Nat. Commun. 4, 1799 (2013).

- <sup>26</sup>L. Liu, T. Moriyama, D. C. Ralph, and R. A. Buhrman, Phys. Rev. Lett. 106, 036601 (2011).
- <sup>27</sup>Z. Qiu and S. Bader, J. Magn. Magn. Mater. **200**, 664 (1999).
- <sup>28</sup>X. Fan, H. Celik, J. Wu, C. Ni, K. Lee, V. O. Lorenz, and J. Q. Xiao, Nat. Commun. 5, 3042 (2014).
- <sup>29</sup>A. Davidson, V. P. Amin, W. S. Aljuaid, P. M. Haney, and X. Fan, preprint arXiv:1906.11772 (2019).
- <sup>30</sup>M. I. Dyakonov, Springer Series in Solid-State Sciences 157: Spin Physics in Semiconductors (Springer, 2008).
- <sup>31</sup>A. Hoffmann, IEEE Trans. Magn. **49**, 5172 (2013).
- 32 T. R. Mcguire and R. I. Potter, IEEE Trans. Magn. 11, 1018 (1975).

- <sup>33</sup>X. Fan, A. R. Mellnik, W. Wang, N. Reynolds, T. Wang, H. Celik, V. O. Lorenz, D. C. Ralph, and J. Q. Xiao, Appl. Phys. Lett. **109**, 122406 (2016).
- 34W. Wang, T. Wang, V. P. Amin, Y. Wang, A. Radhakrishnan, A. Davidson, S. R. Allen, T. J. Silva, H. Ohldag, D. Balzar, B. L. Zink, P. M. Haney, J. Q. Xiao, D. G. Cahill, V. O. Lorenz, and X. Fan, Nat. Nanotechnol. 14, 819 (2019).
- <sup>35</sup>N. Fujita, N. Inaba, F. Kirino, S. Igarashi, K. Koike, and H. Kato, J. Magn. Magn. Mater. 320, 3019 (2008).
- <sup>36</sup>V. Tshitoyan, C. Ciccarelli, A. P. Mihai, M. Ali, A. C. Irvine, T. A. Moore, T. Lungwirth, and A. I. Ferguson, Phys. Rev. B 92, 214406 (2015).
- Jungwirth, and A. J. Ferguson, Phys. Rev. B 92, 214406 (2015).

  37W. Zhang, M. B. Jungfleisch, F. Freimuth, W. Jiang, J. Sklenar, J. E. Pearson, J. B. Ketterson, Y. Mokrousov, and A. Hoffmann, Phys. Rev. B 92, 144405 (2015).